CrossMark

The Effects of Debonding on the Low-Velocity Impact Response of Steel-CFRP Fibre Metal Laminates

T. Pärnänen [1] · A. Vänttinen [2] · M. Kanerva [1] ·
J. Jokinen [1] · O. Saarela [1]

Abstract The effect of metal-composite debonding on low-velocity impact response, i.e. on contact force–central deflection response, deformation profiles and strains on the free surfaces was studied. We focused on type 2/1 fibre metal laminate specimens made of stainless steel and carbon fibre epoxy layers, and tested them with drop-weight impact and quasi-static indentation loadings. Local strains were measured with strain gauges and full-field strains with a 3-D digital image correlation method. In addition, finite element simulations were performed and the effects of debonding were studied by exploiting cohesive elements. Our results showed that debonding, either the initial debonding or that formed during the loading, lowers the slope of the contact force–central deflection curve during the force increase. The debonding formation during the rebound phase was shown to amplify the rebound of the impact side, i.e. to lower the ultimate post-impact deflection. The free surface strains were studied on the laminate's lower surface at the area outside the debond damage. In terms of in-plane strains, debonding formation during impact and indentation, as well as the initial debonding, lowered the peripheral strain and resulted in a positive change in the radial strain.

Keywords Fibre metal laminates · Hybrids · Impact behaviour · Debonding

1 Introduction

The influence of impacts on the load-carrying capability of a structure is one of the prime concerns when the whole lifespan of the structure is considered. Fibre metal laminates (FMLs) are a certain adhesively bonded hybrid laminate concept consisting of fibre-reinforced plastics

✉ T. Pärnänen
tuomas.parnanen@aalto.fi

1   Department of Mechanical Engineering, Aalto University, School of Engineering, PO Box 14300, 00076 Espoo, Finland

2   VTT Expert Services Ltd, PO Box 1001, 02044, VTT, Espoo, Finland

and metal sheets [1]. FMLs were originally developed to perform against fatigue loading. However, they were also found to possess high impact resistance compared to pure metals and composites. Recently, owing to their high bearing strength, steel based FMLs with carbon fibre reinforced plastic (CFRP) layers have been applied to structures with mechanical fastening [2–4]. Also, CFRP laminates with steel and rubber layers have been considered for the impact prone leading edges of airliners' wings [5].

An intrinsic objective of impact engineering is to gain knowledge for designing impact resistant and tolerant laminate structures. A way to gain knowledge is to understand the interaction of the damage modes involved in the full impact damage process (matrix cracking, fibre failure, delamination, debonding and metal cracking). The proper examination for the damage interaction however requires a fundamental understanding of the mechanics and outgrowth of each damage mode, i.e., of the effects of damage modes on the load-deflection response and straining over the laminate.

The relevant literature offers little information on the effects of impact induced debonding on the impact response of FMLs. The cross-sectional images after impact have indicated that debond damage forms under the impact point at the interface of the back wall metal and remaining laminate [6–11]. This particular debonding damage has been shown to form during the impactor withdrawal phase of the impact event [12, 13]. The cross-sectional images have also indicated that debond damage may additionally appear at the upper metal-composite interfaces. The most evident separation is typically found in the surroundings of the impact point rather than under the impact point [6, 7, 14]. Depending on the fibre alignments in the laminate and on the location of the debonded interface, the shapes of the debond damage are something between oval, rectangular and circular [6, 9, 15].

Debonding does not significantly participate in the energy absorption process with practical interface fracture toughness values [16, 17]. However, debonding affects the load transfer between the metal and composite layers, as well as the interaction between different damage modes during an impact, which makes it important in the damage process [12]. Owing to this, debonding has been implemented in the recent theoretical and finite element models in order to study low-velocity impact behaviour [6, 16, 18–20]. However, the models have been utilized to simulate the high-energy impact response of FMLs, which includes all the different damage modes. The interpretation of the sole effects of debonding from the results is, therefore, challenging.

In this research, we investigate the effects of debonding on the low-velocity impact response of steel-CFRP FMLs, i.e. we focus on the contact force–central deflection response, deformation profiles and surface strains. The load response is examined by drop-weight impact and quasi-static indentation tests (see Table 1). In addition, finite element simulations are applied to dissect the sole effects of debonding.

2 Materials and Methods

2.1 The Purpose of the Specimens and FE Simulations

The results of our previous studies revealed that the plastic deformation of the metal layers and debonding are the primary damage modes present in the low-energy impacts of the CFRP-steel FMLs [12]. To study the sole effect of debonding, we now use two different finite element

**Table 1** The experiments and simulations of the research presented in this work

Type of specimen	Impact testing	Indentation testing	FE Simulation
Fully bonded FML, debonding prevented	-	-	No composite damage modes, no strain rate hardening, no debonding
Fully bonded FML	All damage modes in effect	All damage modes in effect, no dynamic effects	No composite damage modes, no strain rate hardening
Initially unbonded FML	All damage modes in effect, debonding emphasized	All damage modes in effect, no dynamic effects, debonding emphasized	-

models, as illustrated in Table 1. The first model only takes into account the plastic deformation of the metal layers. The second model involves the debonding formation as a part of the damage process. To exclude the effect of composite damage and inherent interaction with the debonding formation, we did not model the composite damage. Therefore, the comparison of the results of these two models offers information about the effect of debonding formation on the FML panel's mechanical response.

The exact controlling of debonding formation as well as composite damage in real FMLs is impossible. Therefore, we compare the loading response of traditional FML specimens and initially debonded specimens by experiments (see Table 1). In the initial debonding studies, we use unbonded specimens in which there is no bonding between the metal sheets and the composite part. The comparison of the experimental results provides information on the emphasized effects of debonding on the impact response.

2.2 Specimen Preparation

Test specimens were fabricated of M21/T700GC carbon fibre UD (Hexcel, thickness 0.125 mm) and AISI 304 L stainless steel sheets (Outokumpu Oyj, thickness 0.6 mm). The metal sheets were machined to meet the final specimen dimensions of 110×110 mm^2 prior to the lamination process. The metal rolling direction was set to correspond to the fibre 0° direction. Additionally, epoxy-based adhesive film FM 300NK (Cytec Engineered Materials, thickness 0.15 mm) was applied between the metal sheets and the composite part. The specimens had a [0°/90°/90°/0°] cross-plied composite lay-up and type 2/1 FML stacking (Fig. 1).
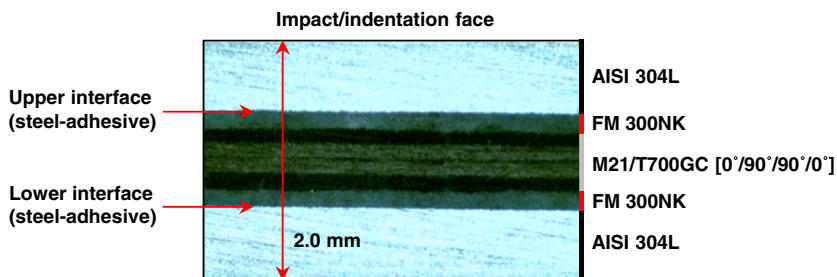
Fig. 1 The lay-up for the bonded and unbonded FML specimens

Two completely different specimens, unbonded and bonded, were prepared. During the lamination of the unbonded specimens, an ethylene tetrafluoroethylene (ETFE) release film was placed between the steel sheets and the adhesive film to prevent any bond from forming. The release film pieces were removed after autoclave curing. As a result, the unbonded specimens consisted of three separate parts, loosely stacked together. The bonded specimens were laminated in a traditional way, without any release film. In order to ensure and control the bonding between stainless steel and the adhesive film, surface treatments were applied according to our previous studies [12, 21]. The surface treatments affect the surface roughness and the level of bonding strength but have a negligible effect on impact behaviour as long as debonding is not the dominating damage mode [12, 22].

The FML specimens were cured in an autoclave (at 177 °C and 2 bar) between two thick aluminium plates to ensure constant temperature distribution through the specimens. The nominal thickness of the cured specimens was 2.0 mm. At this stage of the study, four unbonded and 36 bonded specimens have been manufactured and tested.

2.3 Impact Testing

The impact response was studied by carrying out drop-weight impact testing with a test apparatus described in ASTM D5628–10. The impacts were performed by lifting the impactor (mass 6261 g) to a predefined height and dropping it in a controlled manner. The impact energies were adjusted to range from 10 J to 56 J. A hemispherical steel head (diameter 15.9 mm) was fixed to the impactor. The contact force was measured using a load washer (20 kN) located between the steel head and the impactor mass. The data was recorded at a 180 kHz frequency. The displacement of the impactor was numerically integrated from the measured contact force–time curve (see e.g. [14]).

The bonded and unbonded FML specimens were fixed to the test apparatus by two steel fixtures with a circular, 80 mm diameter test area, as described in Fig. 2. Prior to testing, a release film (ETFE, $t = 0.025$ mm) was placed on the specimen, at the impact point, to stabilize the frictional sliding between the impactor and the steel surface.
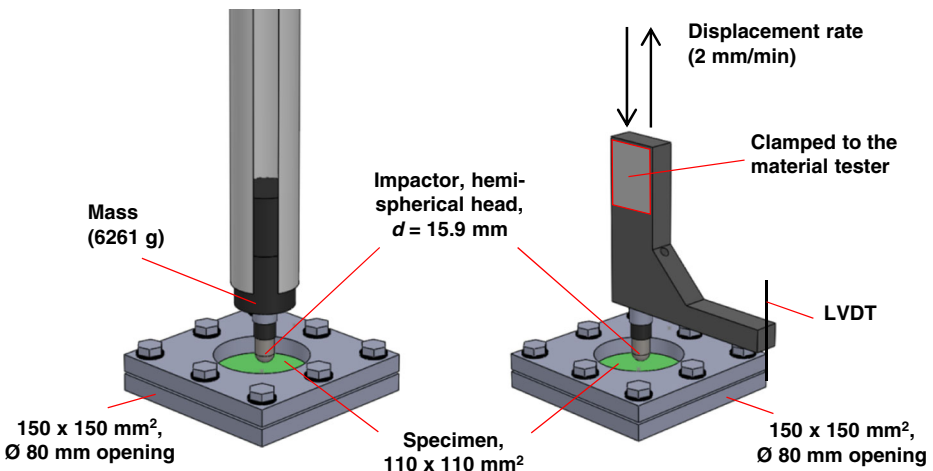

Fig. 2 The drop-weight impact and indentation test set-up schematics

2.4 Indentation Testing

Indentation testing was performed using a servo-hydraulic material tester and followed the guidelines given in ASTM 6264–98. The impactor (indentator) head and the specimen fixtures were similar to the ones used in the drop-weight testing. The indentations were performed at a displacement rate of 2 mm/min. The peak force was set to meet the maximum force of the corresponding impact event. After reaching the peak force (4.9–13.1 kN), the tester was automatically returned to the initial position. The force data was measured with the help of the internal load cell of the material tester (100 kN) and the displacement of the impactor head with an auxiliary displacement transducer (LVDT) fixed to the impactor clamping, as illustrated in Fig. 2. Prior to testing, a release film (ETFE, t = 0.025 mm) was placed on the specimen, at the indentation point, to stabilize the frictional sliding between the impactor and the steel surface.

2.5 Damage Detection

The post-test damage inside the FML specimens was studied using ultrasonic inspection (Omniscan MX, Olympus, Japan). The specimens were scanned underwater using the through-transmission mode and spatial scan resolution of 1 mm/point. C-scan images were produced applying 2.25 MHz transducers of 13 mm diameter. In addition, the deflection profiles of the tested specimens were measured along a line crossing the impact/indentation point in the specimen's lateral (90°) direction. A laser displacement transducer (LK-081, Keyence, Japan) at a 0.25 mm/point spatial resolution was used for this task.

2.6 Full-Field Strain Measurements

The digital image correlation method was used to determine full-field strains on the surface of the impacted FML specimens. A 3-D digital machinery (Aramis, GOM, USA) was applied. A proper speckle pattern was produced on the specimen's lower surface with the help of grey and black spray primers. To measure post-impact strains, a specimen was imaged by using two cameras to take images both prior to and after the impact event while the specimen was attached to the test fixtures, as illustrated in Fig. 3. The strain field images were produced with
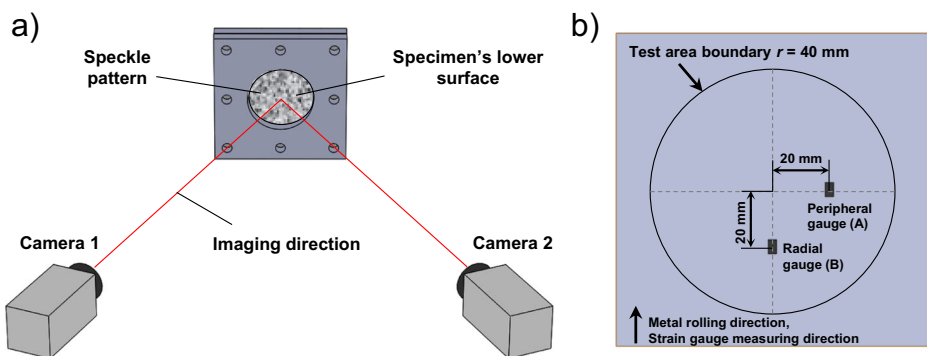

Fig. 3 The Aramis test setup and strain gauge arrangement for strain measurements: **a** specimen's lower surface imaging for the full-field strain determination and; **b** strain gauge locations on the specimen's lower surface for the local strain measurements

the manufacturer's software. The functionality and reliability of the setup was confirmed by several preliminary measurements at different impact energies.

2.7 Local Strain Measurements

Local strains during impact and indentation tests were measured using strain gauges. Two strain gauges (Kyowa, Japan) with a gauge length of 1.0 mm were attached, with the manufacturer's adhesive, on a specimen's lower surface. The gauges were located at a radial distance of 20 mm from the impact/indentation point. The measuring direction for the two strain gauges was set so that peripheral and radial strains were separately measured, as shown in Fig. 3. The data was recorded at 1 kHz frequency during impact testing and at 1 Hz frequency during indentation testing.

2.8 Finite Element Modelling

Finite element (FE) simulations to represent 10 J drop-weight impact and 4.9 kN indentation events were performed using Abaqus 6.14 (Standard). The different layers of the FML structure were modelled using eight-node linear brick elements (C3D8I). A linear-elastic material model was applied for composite and adhesive layers, whereas the Johnson-Cook hardening model ($A = 250$ MPa, $B = 1350$ MPa and $n = 0.7$) was utilized for the steel sheets (see Table 2). Curing residual stresses were taken into account by applying a thermal load prior to mechanical loading ($T_{initial} = 177$ °C and $T_{loading} = 22$ °C). The out-of-plane displacements of the upper and lower surfaces of the specimen outside the test area ($r = 80$ mm) were restrained in order to model the clamped edges during testing. The impactor was first forced to translate a 3.7 mm distance, the maximum displacement found during the 10 J impact experiment, in the out-of-plane direction and then to return to its initial position.

Two different models were created. In the first model (FE-model 1), all the layers were rigidly connected and, therefore, the results represent the laminate response without any debonding. The second model (FE-model 2) included cohesive elements (COH3D8) at the

Table 2 The mechanical properties of the constituent materials used in the FML modelling

Property	Carbon-expoxy UD M21/T700GC	Steel AISI 304 L	Adhesive film FM300NK
Thickness [mm]	0.127	0.6	0.15
Modulus [GPa]	124.9 (E_1)[a], 7.2 (E_2)[a], 7.2 (E_3)	197.5[c]	2.8[f]
Poisson's ratio [−]	0.31 (v_{12})[a], 0.31(v_{13}), 0.38 (v_{23})	0.264[d]	0.4[f]
Shear modulus [GPa]	4.0 (G_{12})[a], 4.0 (G_{13}), 2.6 (G_{23})		
Thermal expansion coeff. [10^{-6}/ ° C]	0.22 (a_1)[b], 40.7 (a_2)[b], 40.7 (a_3)[b]	16.9[e]	48.6[g]

[a] In-house testing (ASTM D3039–00)

[b] Ref [23]

[c] In-house testing (ASTM E111–97)

[d] In-house testing (ASTM E132–04)

[e] Ref [24]

[f] Ref [25] (FM 300 U)

[g] Ref [22] (FM 300 U)

upper and lower steel-adhesive interfaces close to the impactor contact point ($R = 10$ mm). The damage in the cohesive elements was modelled by a bilinear cohesive zone law with a quadratic nominal stress criterion for damage initiation and a power law criterion for damage evolution. The selection of representative material parameters for the cohesive elements ($t_n^0 = 50$ MPa; t_s^0, $t_t^0 = 100$ MPa; K_{nn}, K_{ss}, $K_{tt} = 5 \times 10^{14}$ N/m^3; $G_{IC} = 1750$ J/m^2 [26]; and G_{IIC}, $G_{IIIC} = 3500$ J/m^2 [26]) is reported in our previous work [13]. The global cohesive element size was 0.45 mm. No damage model was applied for the composite part. More details of the modelling and simulation scheme can be found in [13].

3 Results

3.1 The Impact and Indentation Response of the Specimens

The contact force–central deflection curves for impact and indentation loaded specimens are shown in Fig. 4. For all unbonded specimens, the initial stiffness is very low. This is because the individual, detached parts in the specimens possess only minor bending rigidity. However, the specimens become stiffer as the membrane stretching increases in the individual parts. In terms of central deflection, the lack of bonding led to increased (2–24 %) post-test central deflection during impact *and* indentation. The effect of initial debonding on the impact response was similar for 10 J and 56 J specimens, i.e. the initially debonded specimens experienced higher maximum and post-impact deflections. Thus, initial debonding has a clear effect on impact response over a large impact energy regime.

3.2 Internal Damage in Impact and Indentation Loaded Specimens

Typical C-scan images of bonded FML specimens and the composite parts of unbonded specimens after testing are shown in Fig. 5. The white colour in the images represents internal damage, i.e. a combination of different failure modes such as composite damage, debonding and delamination. It is important to note that the C-scans of the bonded specimens do not reliably distinguish debonding and other damage modes in the composite part. The damage in the unbonded specimens gives an estimate of the damage in the composite part per impact energy. For a 10 J impact, the damage in
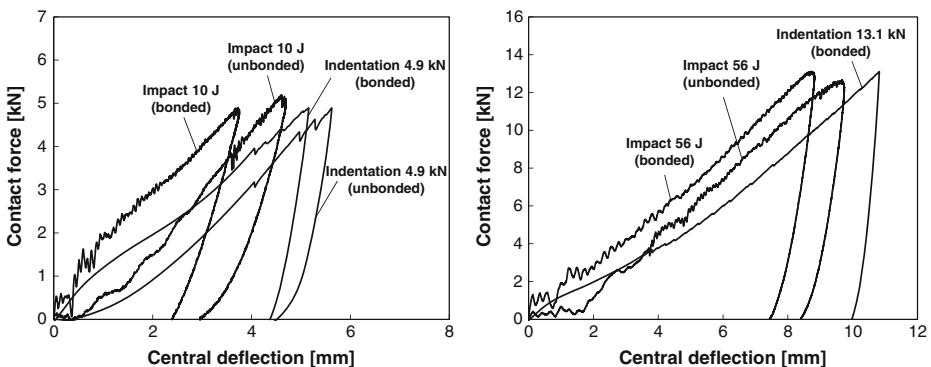

Fig. 4 The contact force–central deflection curves for impact and indentation loaded FML specimens and two different loading levels
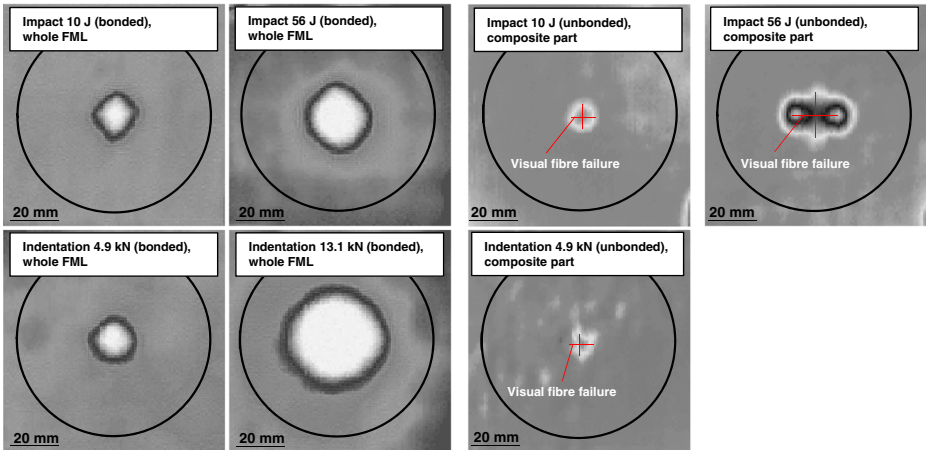
Fig. 5 The C-scan images of impact-loaded and indentation-loaded FML specimens. For unbonded specimens, only the composite parts were scanned

the composite was minor and focused under the impact point ($r < 5$ mm). The internal damage observed from C-scans of indentation loaded specimens was higher compared to impact loaded specimens at a comparable energy. This finding suggests that the debonding damage might be load-rate dependent. In the existing literature, supporting information can be found for load-rate dependent fracture toughness at metal-polymer interfaces [27, 28].

3.3 The Post-Load Deflection Profiles of Bonded and Unbonded Impact Specimens

The deflection profiles of bonded and unbonded FML specimens after a 10 J impact – when the effect of composite damage is low – are shown in Fig. 6. The profiles were in agreement with the maximum (central) deflections determined based on the data of impact testing (Fig. 4). The plastically deformed steel sheets of the unbonded FML specimens had a remarkably higher maximum deflection when compared to the maximum deflection of bonded specimens. The measured deflection profiles clearly point out the differences in the constituent material response. Whereas the elastic-plastic steel sheets have strongly deformed beyond the yield limit (in the plastic strain region), the linear-elastic composite part has experienced only a minor permanent deflection. The deflection of the composite part is due to fibre breakage and adhesive cracking at and around the impact point.
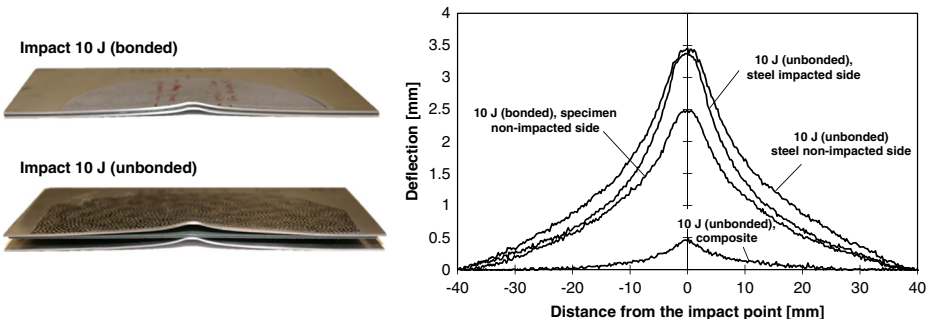

Fig. 6 The cross-sectional images of 10 J impact loaded specimens and their measured post-impact deflection profiles

3.4 Simulated Load Response of the Specimens

The contact force–central deflection curves provided by the two FE simulations are compared with the experimental impact (10 J) and indentation (4.9 kN) results in Fig. 7. It can be seen that, in the early phase of loading, the FE curves closely follow the (time-averaged) FML response measured for impact loading. The lower stiffness measured in the indentation test might be due to slipping of the specimen boundaries at the beginning of the test. When the load increases, the stiffness of the FE models decreases faster than in the impact experiment. Based on the simulations, debonding initiates and progresses along the upper steel-adhesive interface due to interfacial shear forces (see Fig. 7). As a result, the curve slope of the FE-model 2 is slightly decreased when compared to the slope of the FE-model 1. During the unloading, the debonding at the upper interface ceases to propagate. However, debonding initiates at the lower interface and the central deflection clearly decreases during the final part of the unloading step. The lower interface debonding is caused by the peeling force, as the composite part, together with the upper steel sheet, tends towards the initial shape. The size of the debonded area is comparable with the damage sizes measured in the impact and indentation tests (Fig. 5).

In Fig. 8, the deflection profiles after indentation loading (4.9 kN) and impact loading (10 J) are compared with the FE simulation results. It should be noted that the simulations were extended to the maximum impactor displacement measured in the impact test (3.7 mm). From the simulated profiles, the one taking debonding into account (FE-model 2) is closer to the shape of the measured curves.

3.5 Measured and Simulated Strain Distributions

Typical full-field post-impact strains (for a 10 J impact), measured on the non-impacted side, are shown in Fig. 9a in the form of von Mises strains and strains in the direction of the y-axis. The von Mises strains showed a significant peaking at the impact point ($r < 6$ mm). The strain gradients for individual strain components reach values (≈ 0.012/mm) that are too high for strain gauge measurements (with practical grid length) close to the impact point. Therefore, a distance
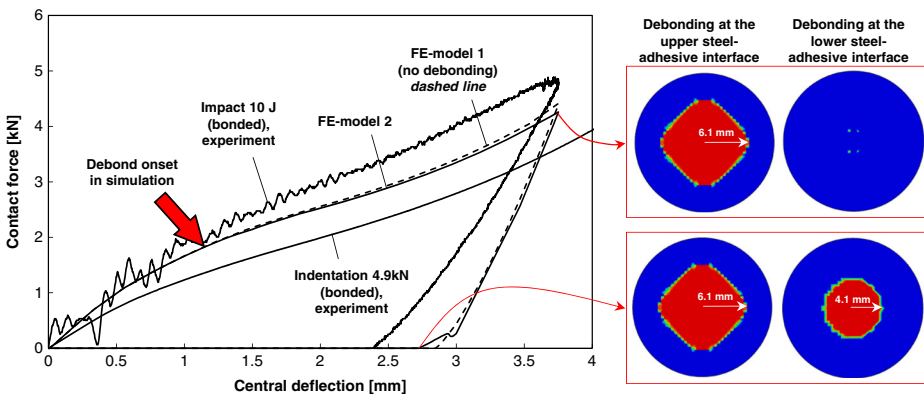

Fig. 7 The contact force–central deflection curves provided by the FE-models and experiments: The debonding damage (SDEG) of FE-model 2 at the upper and lower steel-adhesive interfaces during the loading (the maximum deflection and the end of contact) is represented on the right of the figure. The red-coloured area represents the debonded area. The maximum debond radii from the centre of the specimen are marked by white arrows
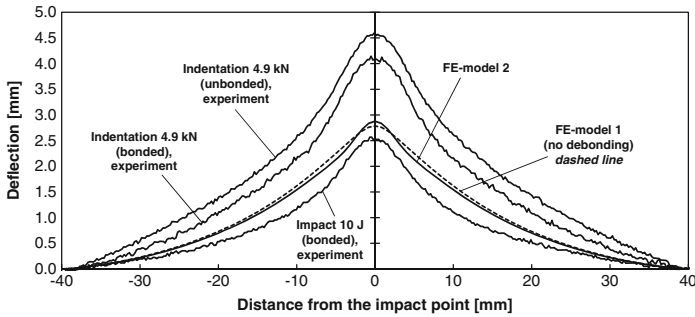
Fig. 8 Deflection profiles provided by the FE simulations and low loading level impact (10 J) and indentation (4.9 kN) tests; the deflections were determined from the lower steel surfaces

of 20 mm from the impact point was selected for the strain gauge measurements. The radial strains were only positive close to the contact point, where the highest strain was far beyond the yield limit of the steel. Outside the contact area, the radial strains were negative, evidencing the bending behaviour of the laminate. The peripheral strain was positive throughout the test area.

Additionally, Fig. 9 represents the results of radial and peripheral strain distributions at the maximum impactor loading and after the impact loading based on the FE simulations, as well as the measured radial and peripheral disributions after the impact. When comparing the simulated maximum strains at the maximum impactor loading, it can be noted that the presence of debonding damage increased the maximum strains encountered by the lower metal layer. The simulation results for the post-impact state suggest that the debonding also increased the maximum post-impact strain at the impact point remarkably.

3.6 Local Post-Impact and Post-Indentation Strains

The post-impact strain (10 J) and post-indentation strain (4.9 kN) of the lower surface, as measured using strain gauges from bonded and unbonded specimens, are shown in Fig. 10. The permanent peripheral strain component was always positive, independent of the bonding and load rates (with impact or indentation tests). However, the peripheral strains were 70–86 % higher after indentation loading when compared to the peripheral strains measured after impact loading.

Independent of the load rate, the measured permanent radial strains were *negative* in the bonded specimens. In turn, the unbonded specimens showed *positive* radial strains after testing. In the unbonded, indentation loaded specimen, the permanent radial strain was six times higher when compared to the unbonded impact loaded specimen. These results indicate that a low rate of loading tends to lead to a more pronounced effect of debonding on permanent strains.

3.7 Strain Build-up during Indentation Loading

The strain build-up during indentation, as measured with the strain gauges and computed with the FE simulations at the same locations, is shown in Fig. 11. The measured peripheral strains were positive through the entire indentation contact, both in bonded and unbonded specimens. In the radial direction, the bonded specimens first encountered negative straining, which indicates that laminate bending took place during the early part of the indentation at the
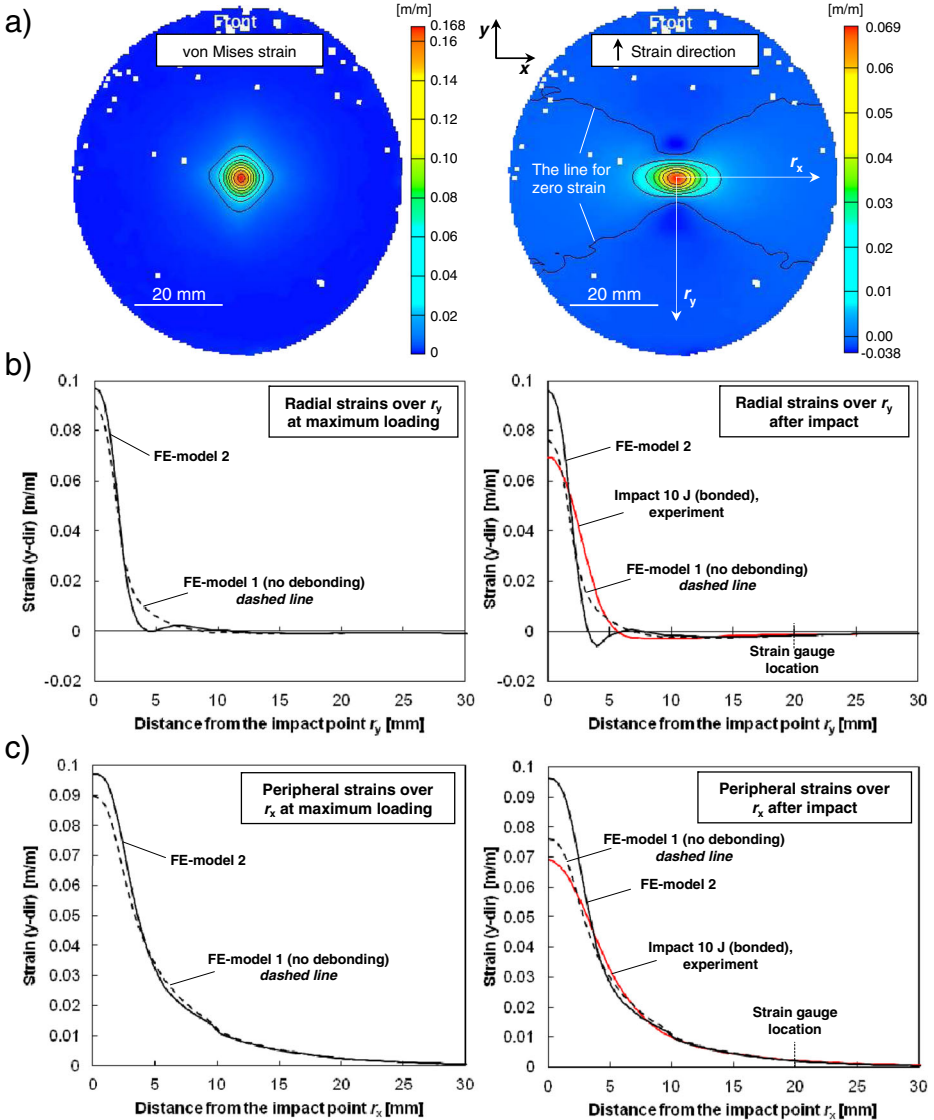
Fig. 9 Strains on the impact specimen's lower surface: **a** the measured post-impact von Mises strain field and y-directional strain field, **b** radial strain distributions at the maximum impactor translation and after the impact and **c** peripheral strain distributions at the maximum impactor translation and after the impact

location of the strain gauges. As the loading increased sufficiently, as it did in the indentation test with the 13.1 kN peak force, the membrane stretching overcame the bending and the radial strain became positive. In the event that the debonding initially existed and covered the entire laminate (meaning the unbonded specimens), the radial strain component turned directly positive, i.e. the specimens only experienced membrane stretching.

The initial bending, as well as the behaviour of the peripheral strain measured for the bonded specimens, was in agreement with the FE simulation results. Based on the simulations,
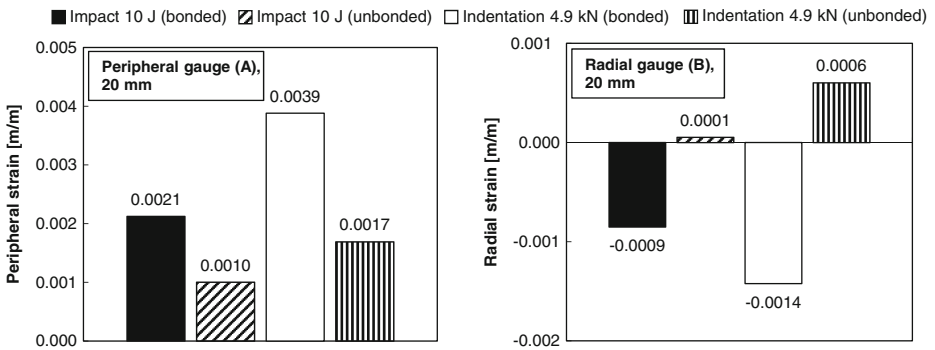
■ Impact 10 J (bonded)   ◪ Impact 10 J (unbonded)   ☐ Indentation 4.9 kN (bonded)   ▥ Indentation 4.9 kN (unbonded)

Fig. 10 The strain gauge post-test strains measured at 20 mm distance from the contact point for 10 J impact and 4.9 kN indentation specimens

natural debonding during the loading does not significantly affect the strain build-up outside the impact point (at the 20 mm strain gauge location).

It is interesting to note that the unloading phase led to a negative radial and peripheral strain change in all the studied cases – even when the radial strain during the indentation was solely negative. This result indicates that the FML specimens were indeed carrying the indentation load chiefly through membrane stretching. Clearly, the elastic part of the membrane strain led to a negative in-plane strain (compression) in the metal sheet on the non-loaded side during the unloading. This is also the reason why the permanent strains in the unbonded specimens were low compared to bonded specimens (Fig. 10), even though the deflections of the unbonded specimens were higher (Figs. 6 and 8). The observed membrane stretching is supported by Morinière et al. [29] who reported that over 96 % of the impact energy is absorbed by the membrane stretching (for Glare 5–2/1 FML) during impact.

4 Discussion

4.1 The Effect of Debonding on the Impact Response

In this work, we studied metal-composite debonding, which occurs during impact and indentation loading of FMLs, to determine its effect on load response and laminate strains.
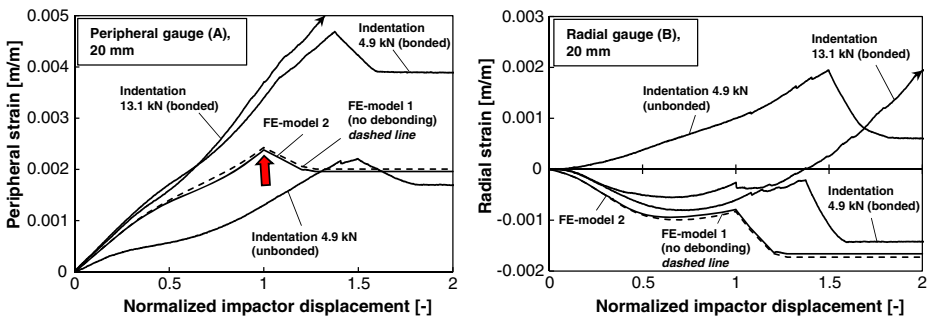

Fig. 11 The peripheral and radial strain build-up during indentation testing and simulations. The strain build-ups are measured and computed 20 mm away from the contact point and on the non-loaded surface of the FML specimens. The cumulative impactor displacement is normalized to the maximum impactor displacement used in FE simulations (3.7 mm). The red arrow shows the initiation of the unloading phase in the FE simulation results

We experimentally compared the impact and indentation response of fully bonded and fully debonded specimens. The unbonded specimens clearly had a lower stiffness, in terms of the slope of the contact force–central deflection curve, in the early part of loading. Based on our FE simulations, load-induced debonding also results in stiffness decrease as the debond forms and expands with the increasing load. In addition, debonding during unloading affects the balance between the cumulated plastic strains and recovering elastic strains, which is shown in the return part of the contact force–central deflection curve. These effects are summarized in Fig. 12.

The effects of debonding depend on whether the debonding occurs at the upper interface or at the lower interface of the type 2/1 FML. The upper interface tends to debond during the loading and, therefore, simulated results are affected by the applied peak force or deflection (the ultimate translation of the impactor). The lower interface tends to debond during the unloading and directly affects the permanent deflection.

We also studied the influence of debonding on the straining of the laminate's lower surface on the area outside the debond damage (20 mm from the impact/indentation point). These results are summarized in Fig. 13. The measured peripheral strains were remarkably lower throughout the contact period in the fully unbonded specimens. The simulation results indicate that the peripheral strain also decreases due to load - induced debonding when compared to the simulation without any debonding damage, though the decrease was small in the simulated case. The radial straining experienced a radical change due to initial debonding. The unbonded specimens experienced positive strains right from the beginning. In turn, bonding between the layers increases the bending rigidity of the FML panel and, therefore, negative straining occurred for the bonded specimens. The change in the radial straining behaviour due to natural debonding, based on the simulations, had a similar tendency as in peripheral straining behaviour, i.e. the strain-displacement curve shifted towards the curve representing strain build-up in the fully unbonded specimen.

4.2 Strain-Rate Strengthening and Stiffening in FMLs

Indentation tests have been used in the current literature to validate indentation models, as well as to support the analysis of low-velocity impact [30, 31]. However, the strain rate is higher for an impact loading compared to quasi-static indentation. Since the (absolute) values of peripheral strains are in general higher than radial strains, the strain rate effects are expected to be more pronounced on the peripheral strain build-up. Anyhow, the strains due to an impact
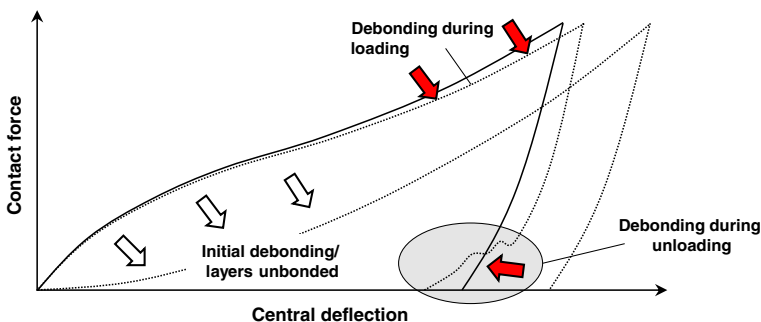

Fig. 12 The effects of initial debonding (*white arrows*) and load-induced debonding (*red arrows*) on the load response of an impact/indentation test specimen
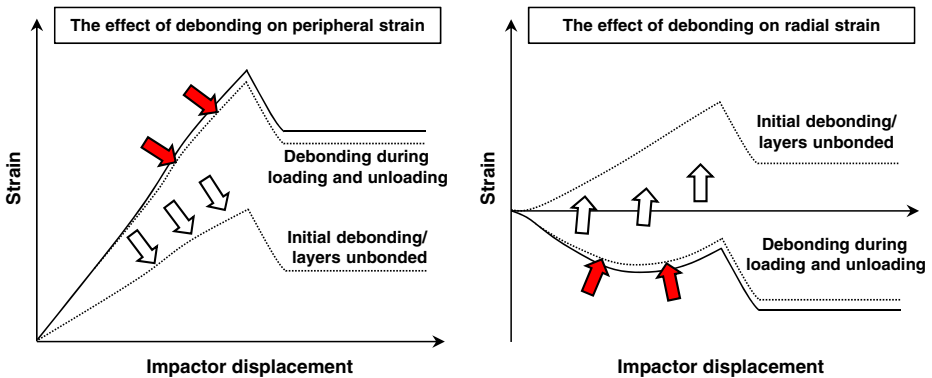
Fig. 13 The effects of initial debonding (*white arrows*) and load-induced debonding (*red arrows*) on the straining of the specimen's lower surface outside the debond damage

accumulate at the impact point, i.e. strain localization occurs, and subsequently the strain rates are high enough to affect mechanical behaviour mostly at the impact point (see Fig. 9). Outside the impact point, the strain build-up during an impact is expected to essentially follow the curves found by quasi-static indentation (see Fig. 11).

A coarse estimate of the maximum strain rates during the impacts in our study was 0.6 s^{-1} based on the strain gauge data measured at 20 mm distance from the impact point. At the impact point, a rough and conservative estimate for the average strain rate is about 21 s^{-1}, based on the y-directional strain field results in Fig. 9 (the peak post-strain being 0.069 m/m and the loading period of the impact being 3.3 ms). Blandford et al. [32] have studied the effect of strain rate on the mechanical properties of AISI 304 L stainless steel. They concluded that the yield point increases ≈40–60 % at a strain rate range of $25–50 \text{ s}^{-1}$ when compared to quasi-static test results. Similar effects of strain rate on the mechanical properties have been observed for carbon fibres too. However, the strain rate stiffening of carbon fibres mostly occurs at a very high strain rate ($>10^3 \text{ s}^{-1}$) [33]. Even though the carbon fibres in our study did not encounter strain rate stiffening, the strain rate stiffening of the steel sheets may cause an increase in the contact force–central deflection curve slope during impact loading. This type of change was also seen in the results between simulation and impact testing (Fig. 7).

Vlot [34, 35] has suggested that fibres with a strong tendency for strain rate strengthening (an increase in ultimate strain due to the strain rate) should be preferred in FMLs to improve impact resistance. Due to the strong localization of strains at the impact point, any fibre failure tends to initiate right at the impact point. Therefore, in addition to strain rate strengthening, it would be beneficial to prefer fibres and metals with a strong tendency for strain rate stiffening (an increase in Young's modulus and yield point). Because the strain rates are highest at the impact point, local stiffening of fibres and metal could transfer load bearing further away and postpone local damage and perforation.

5 Conclusions

We have analysed the effect of metal-composite debonding on the low-velocity impact response of a type 2/1 FML made of stainless steel and carbon fibre epoxy layers. The results of the experiments and FE simulations showed that the debonding decreases the curve slope of

the contact force–central deflection curve during the loading phase of the impact. The simulation results also indicated that debonding formation during the unloading phase influences the end part of the contact force–central deflection curve by amplifying the rebound, i.e. decreasing the final deflection.

The straining of the FML panels outside the region of the debonding damage was our primary interest. The results indicated that debonding formation during impact and indentation, as well as initial debonding, will decrease the peripheral strain and result in a positive change in the radial strain on the panel's lower surface. The effect can be observed during contact, as well as from the permanent strains of the specimen. The change in the straining is partly due to a decrease in bending stiffness and, consequently, an increase in membrane stretching. This research indicates that debonding damage in FMLs loaded by low-velocity impact has an apparent effect on a panel's deflection response and strains, and consequently also on the internal stress state. Therefore, debonding is an important factor in the damage process of FMLs and the debonding should be taken into account in the modelling with its all features.

References

1. Vlot A., Alderliesten R.C.: Fiber metal laminates, fatigue of. In: Buschow K.H.J., Cahn R.W., Flemings M.C., Ilschner B., Kramer E.J., Mahajan S., Veyssière P. (eds.) Encyclopedia of Materials: Science and Technology, second edn, pp. 1–4. Elsevier, Oxford (2001)
2. Hühne, C., Petersen, E.: Fiber-metal-laminates. In: Proceedings of the 13th European Conference on Spacecraft Structures, Materials & Environmental Testing (ESA SP-727), Braunschweig (2014)
3. Kolesnikov B., Stefaniak D., Wölper J., Hühne C.: Payload adapter made from fiber-metal-laminate struts. In: Wiedemann M., Sinapius M. (eds.) Adaptive, Tolerant and Efficient Composite Structures, pp. 263–274. Springer-Verlag, Berlin Heidelberg (2013)
4. van Rooijen R.G.J.: Bearing Strength Characteristics of Standard and Steel Reinforced GLARE. Delft University of Technology, The Netherlands, Dissertation (2006)
5. Düring D., Weiß L., Stefaniak D., Jordan N., Hühne C.: Low-velocity impact response of composite laminates with steel and elastomer protective layer. Compos. Struct. **134**, 18–26 (2015)
6. Nakatani H., Kosaka T., Osaka K., Sawada Y.: Damage characterization of titanium/GFRP hybrid laminates subjected to low-velocity impact. Compos. A: Appl. Sci. Manuf. **42**, 772–781 (2011)
7. Fan J., Cantwell W., Guan Z.: The low-velocity impact response of fiber-metal laminates. J. Reinf. Plast. Compos. **30**, 26–35 (2011)
8. Pärnänen T., Alderliesten R., Rans C., Brander T., Saarela O.: Applicability of AZ31B-H24 magnesium in fibre metal laminates – an experimental impact research. Compos. A: Appl. Sci. Manuf. **43**, 1578–1586 (2012)
9. Wu G., Yang J., Hahn H.T.: The impact properties and damage tolerance and of bidirectionally reinforced fiber metal laminates. J. Mater. Sci. **42**, 948–957 (2007)
10. Seyed Yaghoubi A., Liu Y., Liaw B.: Stacking sequence and geometrical effects on low-velocity impact behaviors of GLARE 5 (3/2) fiber–metal laminates. J. Thermoplast. Compos. Mater. **25**, 223–247 (2011)
11. Yarmohammad Tooski M., Alderliesten R.C., Ghajar R., Khalili S.M.R.: Experimental investigation on distance effects in repeated low velocity impact on fiber–metal laminates. Compos. Struct. **99**, 31–40 (2013)
12. Pärnänen T., Kanerva M., Sarlin E., Saarela O.: Debonding and impact damage in stainless steel fibre metal laminates prior to metal fracture. Compos. Struct. **119**, 777–786 (2015)
13. Pärnänen, T., Jokinen, J., Kanerva, M., Saarela, O.: Debonding modelling of indentation loaded fibre metal laminates. In: Proceedings of the 10th International Conference on Composites Science and Technology, Lisbon (2015)

14. Laliberté J.F.: Investigation of Low-Velocity Impact Damage in Fibre-Metal-Laminates. Carleton University, Canada, Dissertation (2002)
15. Morinière F.D.: Low-Velocity Impact on Fibre-Metal Laminates. Delft University of Technology, The Netherlands, Dissertation (2014)
16. Morinière F.D., Alderliesten R.C., Sadighi M., Benedictus R.: An integrated study on the low-velocity impact response of the GLARE fibre-metal laminate. Compos. Struct. **100**, 89–103 (2013)
17. Hoo Fatt M.S., Lin C., Revilock Jr. D.M., Hopkins D.A.: Ballistic impact of GLARE™ fiber–metal laminates. Compos. Struct. **61**, 73–88 (2003)
18. Tsartsaris N., Meo M., Dolce F., Polimeno U., Guida M., Marulo F.: Low-velocity impact behavior of fiber metal laminates. J. Compos. Mater. **45**, 803–814 (2011)
19. Liu Y., Yaghoubi A., Liaw B.: Low-velocity impact study on GLARE FMLs using various indenters. J. Aerosp. Eng. **27**, 325–335 (2014)
20. Asaee Z., Taheri F.: Experimental and numerical investigation into the influence of stacking sequence on the low-velocity impact response of new 3D FMLs. Compos. Struct. **140**, 136–146 (2016)
21. Kanerva M., Sarlin E., Campbell J.M., Aura K., Saarela O.: Variation in mode II dominated interface fracture of stainless steel-epoxy bonds. Part 2: Multi-scale damage analysis. Eng. Fract. Mech. **97**, 244–260 (2013)
22. Kanerva M., Sarlin E., Saarela O.: Variation in mode II dominated interface fracture of stainless steel-epoxy bonds. Part 1: Mechanical testing. Eng. Fract. Mech. **99**, 147–158 (2013)
23. Nawab Y., Jacquemin F., Casari P., Boyard N., Borjon-Piron Y., Sobotka V.: Study of variation of thermal expansion coefficients in carbon/epoxy laminated composite plates. Compos. B – Eng. **50**, 144–149 (2013)
24. Outokumpu: Type 304, Type 304 L UNS S30400, UNS S30403: The basic austenitic stainless steel, a versatile corrosion resistant material for general purpose applications. Datasheet (2013)
25. Kanerva M., Saarela O.: X-ray diffraction and fracture based analysis of residual stresses in stainless steel-epoxy interfaces with electropolishing and acid etching substrate treatments. Int. J. Adhes. Adhes. **39**, 60–67 (2012)
26. Russell A.J.: A Damage Tolerance Assessment of Bonded Repairs to CF-18 Composite Components. Part I: Adhesive Properties. DREP-Technical Memorandum. 88–25 (1988)
27. Gent A., Schultz J.: Effect of wetting liquids on the strength of adhesion of viscoelastic material. J. Adhes. **3**, 281–294 (1972)
28. Kanerva M.: Strength of Rough Interfaces: A Micro-Scale Approach to Steel-Epoxy and Composite Systems. Aalto University, Finland, Dissertation (2015)
29. Morinière F.D., Alderliesten R.C., Benedictus R.: Low-velocity impact energy partition in GLARE. Mech. Mater. **66**, 59–68 (2013)
30. Bikakis G.S.: FEM analysis and analytical formulas to predict the indentation response of circular simply supported GLARE plates. J. Compos. Mater. **49**, 2459–2468 (2014)
31. Vlot A.: Low-Velocity Impact Loading on Fibre Reinforced Aluminium Laminates (ARALL) and Other Aircraft Sheet Materials. Delft University of Technology, The Netherlands, Dissertation (1991)
32. Blandford R., Morton D., Rahl T., Snow S.: Impact Testing of Stainless Steel Materials. In: Proceedings of ASME Pressure Vessels and Piping, Division Conference, Denver (2005)
33. Davies G.A.O., Olsson R.: Impact on composite structures. Aeronaut. J. **108**, 541–563 (2004)
34. Vlot, A., Krull, M.: Impact damage resistance of various fibre metal laminates. J. Phys. IV 7, C3–1045-C3–1050 (1997)
35. Vlot A., Kroon E., La Rocca G.: Impact response of fiber metal laminates. Key Eng. Mater. **141–143**, 235–276 (1998)